International Journal of Biochemistry and Cell Biology 114 (2019) 105566

Contents lists available at ScienceDirect

International Journal of Biochemistry and Cell Biology

journal homepage: www.elsevier.com/locate/biocel

Chlorogenic acid- loaded calcium phosphate chitosan nanogel as biofilm degradative materials

Subitha Palaniraj, Ramachandran Murugesan, Shoba Narayan*

Faculty of Allied Health Sciences, Chettinad Hospital and Research Institute, Chettinad Academy of Research and Education, Kelambakkam, Tamilnadu, 603103, India

ARTICLE INFO

Keywords:
Restorative dentistry
Re-mineralization
Biofilm
Calcium phosphate
Chitosan
Chlorogenic acid
Nanogel

ABSTRACT

This work describes an effort to develop an antimicrobial agent (chlorogenic acid - CGA) loaded porous nanogel based on calcium phosphate-chitosan (CaPNP@Chi) nanogel with biofilm degradative properties and has potential applications in restorative dentistry. The nanogel was prepared by ionic gelation of calcium phosphate nanoparticles and chitosan in the ratio of 1.25: 1. Chlorogenic acid was loaded to the nanoparticles as an ethanolic solution and the encapsulation efficiency determined by chromatographic techniques. The particle size and morphology of CaPNP@Chi and CaPNP@Chi@CGA was determined by dynamic light scattering and scanning electron microscopic techniques. The minimum inhibitory concentration against *S. aureus and K. pneumoniae* was determined through the well diffusion method. The biofilm formation and biofilm decay were studied through staining assays. The toxicity, if any of the nanogel was assessed by MTT assay against HaCaT cells. All data were statistically analyzed. The composite had a CGA encapsulation efficiency of 70% and was thermally stable up to 124 °C. The zone of inhibition was found to be 18.7 mm ± 0.6 against *S. aureus*. CaPNP@Chi@CGA showed a 68% increase in biofilm degradation when compared with the untreated group. Results obtained in this study suggest that the positively charged nanogel interacted with the bacterial cell membrane and brought about the disruption of the cell membrane. Also, CaPNP@Chi@CGA was observed to be nontoxic up to 40 µg/mL to HaCaT cells. These results support the potential of CaPNP@Chi@CGA nanogel for biofilm degradation and its application as filling material in restorative dentistry.

1. Introduction

Dental caries and periodontal disease are biofilm dependent oral diseases affecting humankind (Tove and Nils-Erik, 2017). Caries involves the adherence of bacteria on the tooth surface as a community of cells embedded in a matrix of extracellular polymers, called biofilm. Failure of dental restoration is associated with acid production promoted secondary caries at the restoration margins (Melo et al., 2013), (Wang and Ren, 2017). Patients with periodontitis compared to the healthy group, are reported to have a significant incidence of *Staphylococcus aureus, Klebsiella pneumoniae,* and *Pseudomonas aeruginosa* infection (Scannapieco and Mylotte, 1996). Strategies to control caries could include a) inhibition of biofilm development through bacteria attachment b) arresting or controlling cell signaling pathway, c) multifunctional therapy by using an appropriate choice of antimicrobials and d) triggering host defense process. Researchers worldwide are working to develop nanomaterials that can stimulate either or all of such process. Resin composites have received attention recently due to their aesthetics and direct-filling capability coupled with bonding agents for cavity restorations. There is considerable interest to develop composites that can fight biofilms and help in remineralization of tooth lesions. Chemical similarities to the bone and teeth make CaP a desired material of choice. Also, CaP cement is biocompatible, resorbable, and has a macroporous structure with micropores that can promote cell growth and infiltration (Cheng et al., 2012). Research on restorative dentistry involves the use of calcium phosphate particles of different nanoformulation that can enhance the efficacy of CaP (Zaltsman et al., 2017). Calcium phosphate in various structural forms like crystalline, amorphous, porous, etc., can be synthesized as gels or composites or cement or as a coating material in dental applications (Pepla et al., 2014). The treatment strategies that use calcium phosphate include the capping of pulp, barrier formation in the apical region, triggering mechanism of dentin etc. For restorative dentistry, combination of polymers, ceramics and metals can lead to a material of biodegradability with superior property (Dias et al., 2019; Venkatesan and Kim, 2014). Among many polymers of biological origin, chitosan forms a resourceful material with its attractive features such as the rich amine groups that aid in mucosal adhesion (Aijun et al., 2006) and

* Corresponding author.
E-mail addresses: shobulu@gmail.com, shobanarayan@chettinadhealthcity.com (S. Narayan).

https://doi.org/10.1016/j.biocel.2019.105566
Received 10 April 2019; Received in revised form 20 June 2019; Accepted 4 July 2019
Available online 05 July 2019

Table 1
Size distribution and zeta (ζ) potential of the synthesized nanogel studied by DLS at pH 7.4 and at salivary pH 6.7.

Samples	pH 7.4 D_H (nm)	pH 6.7 D_H (nm)	pH7.4 ζ-potential (mV)	pH 6.7 ζ-potential (mV)
Uncalcinated CaPNP	329.3 ± 3.61	362.3 ± 2.25	−7.15 ± 0.30	−4.39 ± 0.47
Calcinated CaPNP	76.3 ± 1.36	81 ± 0.89	−11.1 ± 0.25	−6.45 ± 0.16
CaPNP@Chi	559.6 ± 8.5	452.6 ± 2.73	8.58 ± 0.46	20.16 ± 0.68
CaPNP@Chi@CGA	468 ± 2.68	439 ± 0.89	7.06 ± 0.10	18.9 ± 0.32

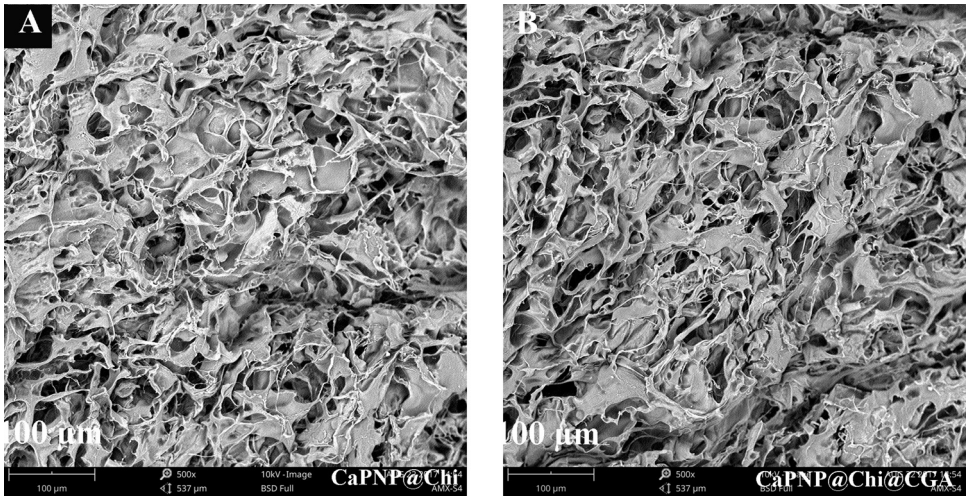

Fig. 1. SEM analysis of synthesized nanogel (A) CaPNP@Chi, (B) and CaPNP@Chi@CGA at 500 X magnification.

antibacterial property against *S. mutans* and other *Streptococci.* The wide range of antimicrobial action of chitosan and its efficacy against different microbial species are well documented (Yiwen et al., 2018). The appealness of chitosan has resulted in its incorporation in mouth wash, tooth pastes, gels, etc. Another essential feature for the multi-functional approach of scaffolds or gel is the presence of pores that can aid in cell adhesion, interaction, and sustained drug release (Roohani-Esfahani et al., 2016). The present study focuses on the development of a porous nanogel that could inhibit bacterial cell adhesion as well as in re-mineralization. The choice of CGA was due to its antibacterial effect, which can exert the intracellular potential, and release cytoplasm contents of the bacteria resulting in cell death (Lou et al., 2011). CGA is useful for preventive dental caries (Petti and Scully, 2009) and is a secondary phenolic metabolite in plants that exists widely in nature, with cardioprotective, lipid-lowering, antioxidant, neuroprotective, lowering blood sugar levels and anti-inflammatory properties (Nallamuthu et al., 2015). Earlier reports on the antibacterial property of CGA encapsulated chitosan nanoparticles have shown the potential of CGA. However for restorative dentistry both re-mineralization and antibiofilm activity are required. Hence in this study, an attempt is made to prepare porous nanogel of CGA loaded CaPNP@Chi and evaluate its potential.

2. Materials and methods

2.1. Materials

All Chemicals used in this work were procured from Sigma Aldrich and/or Himedia, India and were of analytical grade, and used as received without further purification. Bacterial strains, *Staphylococcus aureus, Klebsiella pneumoniae* and *Pseudomonas aeruginosa* were gifted by Department of Microbiology, Chettinad Hospital and Research Institute.

2.2. Synthesis of calcium phosphate nanoparticle

Calcium phosphate nanoparticle (CaPNP) was synthesized following earlier methods with slight modifications (Danilchenko et al., 2011). To a solution of 0.86 M calcium nitrate tetra hydrate (pH 10), 0.65 M diammonium hydrogen phosphate solution (pH 10) was added drop wise under stirring (stoichiometric ratio of calcium to phosphate = 1.33:1). Stirring was continued for 2 h and the solution was left undisturbed for 24 h. The supernatant was removed; the precipitate was washed repeatedly using milli Q water to remove unbound ions and dried at 100 °C for one hour, calcinated.

2.3. Fabrication of calcium phosphate/chitosan nanogel

Fabrication of CaPNP@Chi was done by ionic gelation method using synthesized calcium phosphate nanoparticle as cross-linker. Different amounts of chitosan varying from 1 to 5 mg (dissolved in 1% glacial acetic acid) were used, for the preparation of CaPNP@Chi nanogel. The solution was stirred for 2 h, followed by centrifugation at 3000 rpm for 20 min. The solution was washed repeatedly with milli Q water to obtain CaPNP@Chi nanogel. According to the hydrodynamic diameter of obtained gel, Gel formation was observed at 5 mg of CaPNP and 4 mg of chitosan was chosen.

2.4. Preparation of CGA encapsulated CaPNP@Chi nanogel

CGA entrapped CaPNP@Chi nanogel (CaPNP@Chi@CGA) was prepared by ionic entrapment method as described earlier (Fan et al., 2012) with slight modifications. To 5 mL solution of CaPNP@Chi (5 mg CaPNP and 4 mg chitosan), a solution of CGA (5 mg dissolved in 70% ethanol) was added drop wise under stirring. The solution obtained after stirring for 2 h was washed, centrifuged at 3000 rpm for 20 min. Nanogel was purified and CGA encapsulation efficiency, physiochemical, biological and antimicrobial characterization of the nanogel were carried out in accordance with reported procedures (Shamaila et al.,

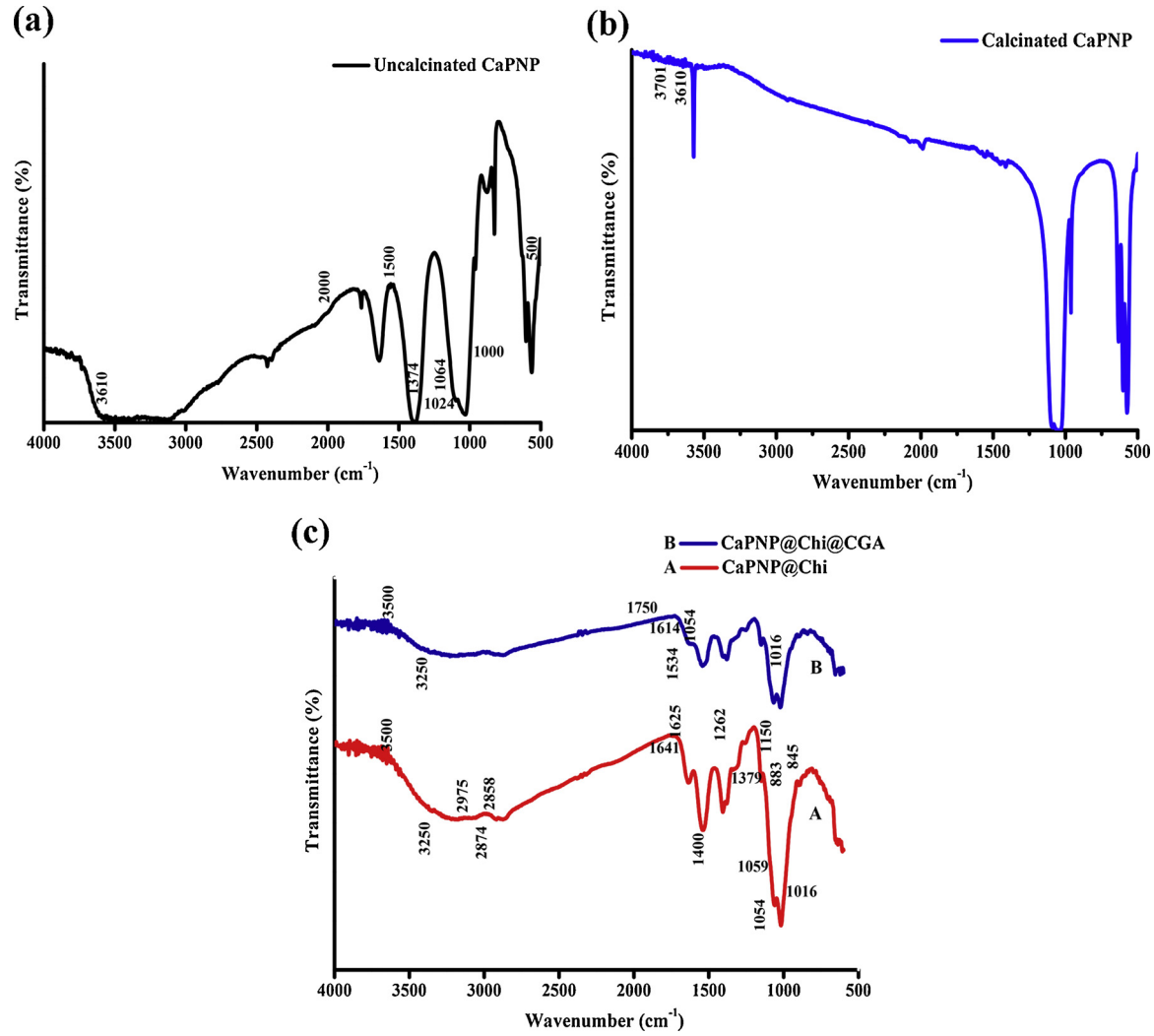

Fig. 2. FTIR spectra of (a) uncalcinated CaPNP, (b) calcinated CaPNP, (c) CaPNP@Chi and CaPNP@Chi@CGA.

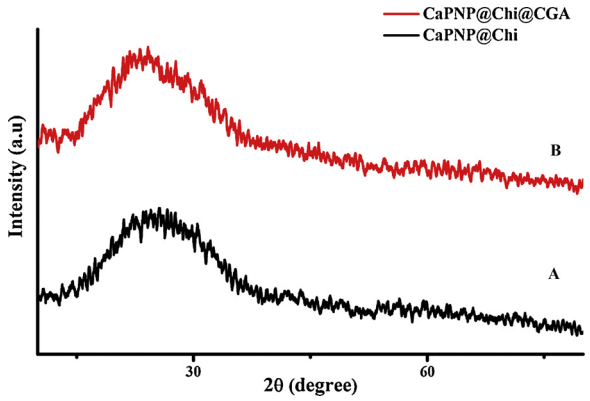

Fig. 3. XRD pattern of CaPNP@Chi and CaPNP@Chi@CGA.

2016) (Baidamshina et al., 2017; Ommen et al., 2017) (Chen et al., 2013) (Wang et al., 2015).

2.5. Physiochemical characterization of CaPNP@Chi@CGA nanogel

Dynamic Light Scattering (DLS) was used to measure the hydrodynamic size of particles in solution through Malvern Zetasizer Nano ZS instrument. To understand the surface charge and stability of nanogel, these samples were further subjected to zeta potential measurements. The drug encapsulation efficiency in the nanogel was determined by High Performance Liquid Chromatography (HPLC). For this the amount of free CGA present in the supernatant was determined. Phenomenoxgemin 5 µm (150 × 4.6 mm) column was used with the mobile phase consisted of 30% acetonitrile and 0.6% ortho-phosphoric acid. The system was run dramatically with a flow rate of 5 min, 10 µL of the sample was injected into the column and quantification was done at 325 nm using photo diode array detectors.

Scanning Electron Microscopic evaluation (SEM) was performed to understand the surface morphology and porous structure of nanogel. For this the samples were separated by centrifugation at 3000 rpm for 30 min. The supernatant of the samples were discarded and the pellets were lyophilized. The lyophilized pellets were examined by SEM. Fourier Transform Infrared Spectroscopy (FTIR) was used to determine the adsorption/entrapment of drugs in nanogel. The crystalline phases and diffraction patterns of precipitated and lyophilized nanogel was confirmed by X-Ray Diffraction (XRD). Differential Scanning Calorimetry (DSC) was used to determine the energetics of phase transitions of CaPNP@Chi@CGA. The thermal stability of CaPNP@Chi@CGA as a function of temperature was studied by Thermogravimetric Analysis (TGA).

2.6. Biological characterization of CaPNP@Chi@CGA nanogel

The synthesized nanogel CaPNP@Chi@CGA was tested for

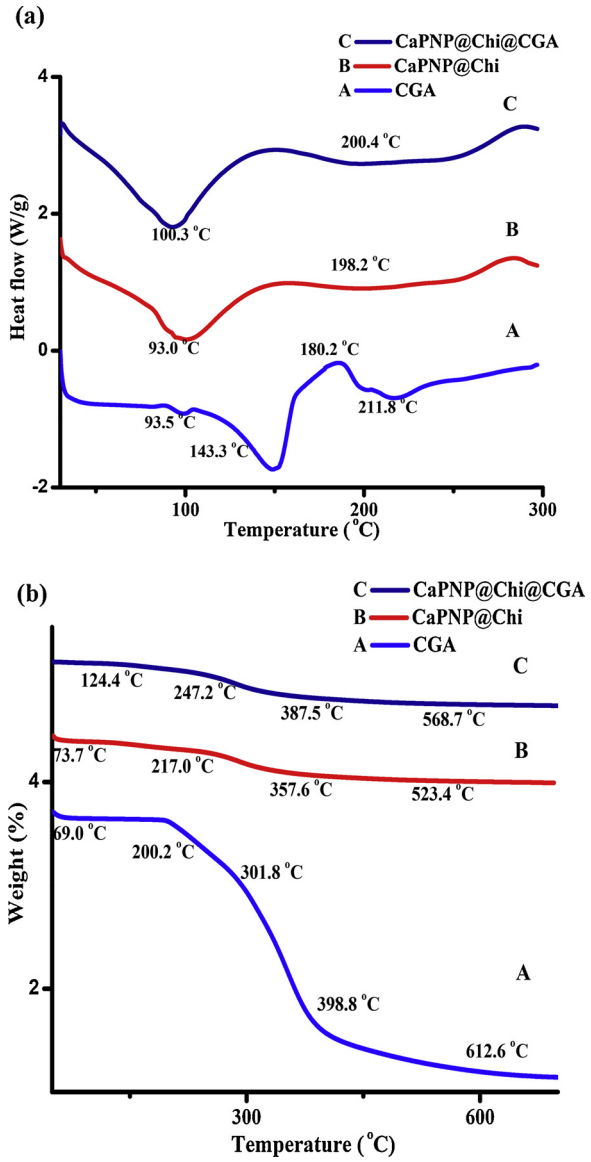

Fig. 4. (a) DSC and (b) TGA analysis of (A) CGA, (B) CaPNP@Chi and (C) CaPNP@Chi@CGA.

minimum inhibitory concentration for antibacterial potential by well diffusion method. Biofilm degradation was assessed by crystal violet and safranin O staining assay. Bacterial cellular morphology was analyzed by HR SEM and cytotoxicity assay by MTT.

2.6.1. Evaluation of antibacterial activity by well diffusion method

The minimum inhibitory antibacterial potential from the varying concentration of CGA (1–15 μg) of CaPNP@Chi@CGA nanogel was evaluated by well diffusion method on nutrient agar for two bacterial strains (*S. aureus and K. pneumoniae*). The inhibitory antibacterial potential of CGA (20 μg) of CaPNP@Chi@CGA nanogel against *Pseudomonas aeruginosa* was evaluated. The nutrient agar plate was inoculated by spreading a volume of bacterial inoculum over entire agar surface under aseptic conditions. Then a hole with 4 mm was created using sterile cork borer, 50 μL of the sample was loaded into the well and incubated at 37 °C for 24 h. After the incubation, the material diffuses in the agar medium and inhibits the bacterial growth and zone of inhibition was measured in mm.

2.6.2. Biofilm formation

Bacterial suspension of 100 μL was inoculated in nutrient broth and incubated at 37 °C for 24 h. The inoculated bacterial suspension of 100 μL (5000) cfu was added to each well and incubated at 37 °C for 24 h in a sterile flat bottomed 96 well polystyrene microtitre plates, to permit bacterial adhesion and biofilm formation on surfaces. After the incubation, the supernatant was discarded and the non-attached bacterial cells was washed two times using 100 μL of 0.9% (W/V) NaCl. Remaining biofilms were treated with 50 μL of nutrient broth containing with or without 50 μL of nanogel (Control, CaPNP, CaPNP@Chi, CGA and CaPNP@Chi@CGA) incubated at 37 °C for 24 h. Biofilm incubated only with nutrient broth was used as a control. After incubation, supernatant containing non-attached cells were washed two times using 100 μL of 0.9% (W/V) NaCl. The biofilm attached in the wells were fixed using 100 μL of methanol for 20 min. The plates were dried out for 20 min at RT.

2.6.3. Crystal violet and safranin O staining assay: Biofilm degradation assay

Biofilm mass was evaluated by crystal violet (gram positive) and safranin O staining assay (gram negative) in accordance with previous procedure. For the crystal violet staining assay, samples in the wells (control and treated) were stained with 100 μL of 1% crystal violet and retained for 20 min at RT. Then the crystal violet was removed and plates were washed three times using deionized water. Stained biofilm was then solubilized using 150 μL of 1% acetic acid. The biofilm mass were measured at 590 nm in microplate reader. Same procedure has been performed for gram negative bacteria by safranin O staining assay. Plates were measured at 550 nm using microplate reader.

2.6.4. Scanning electron microscopic analysis: biocidal activity

The morphology of the biofilm was observed by HRSEM. For biofilm formation on coverslip, same method was adopted, which was previously explained. Control and treated samples CaPNP@Chi@CGA were fixed using 1 mL of 2.5% glutaraldehyde and kept at 4 °C for 24 h. Bacterial cells were washed three times using 1 mL of 1X PBS at each time interval. Cells were dried out using different concentration of alcohol for 10 min. Coverslips were mounted onto aluminum stub with carbon tape, sputter coated with gold for the HRSEM analysis.

2.6.5. Cytotoxicity assay by MTT

Cell viability of HaCaT cells upon incubation with nanogel CaPNP@Chi@CGA was estimated through MTT assay. HaCaT cell line was grown in DMEM supplemented with 10% FBS, 100 μg/mL penicillin and 100 μg/mL streptomycin at 37 °C in a 5% CO_2 incubator. Cells were grown to reach 70–80% confluence. 200 μL of cells containing 5×10^3 cells were incubated at 37 °C for 12 h in 96 well plates. The medium was replaced with the fresh medium containing different concentration of CaPNP@Chi@CGA (10, 20, 30 and 40 μg/mL) and incubated at 37 °C for 18 h in triplicate. Cells incubated in the medium containing no nanogel were used as control. After 18 h of incubation, 10 μL of MTT reagent (5 mg/mL) was added to each well and incubated for 4 h in a dark room. Medium was removed after the incubation and 100 μL of DMSO was added to each well to solubilize formazan crystals. The purple color was observed. The plate was read at 570 nm using microplate reader

2.7. Statistical analysis

The results were expressed as the mean ± SD. The values were calculated based on the student's t-test, and $p < 0.05$ was considered as statistically significant.

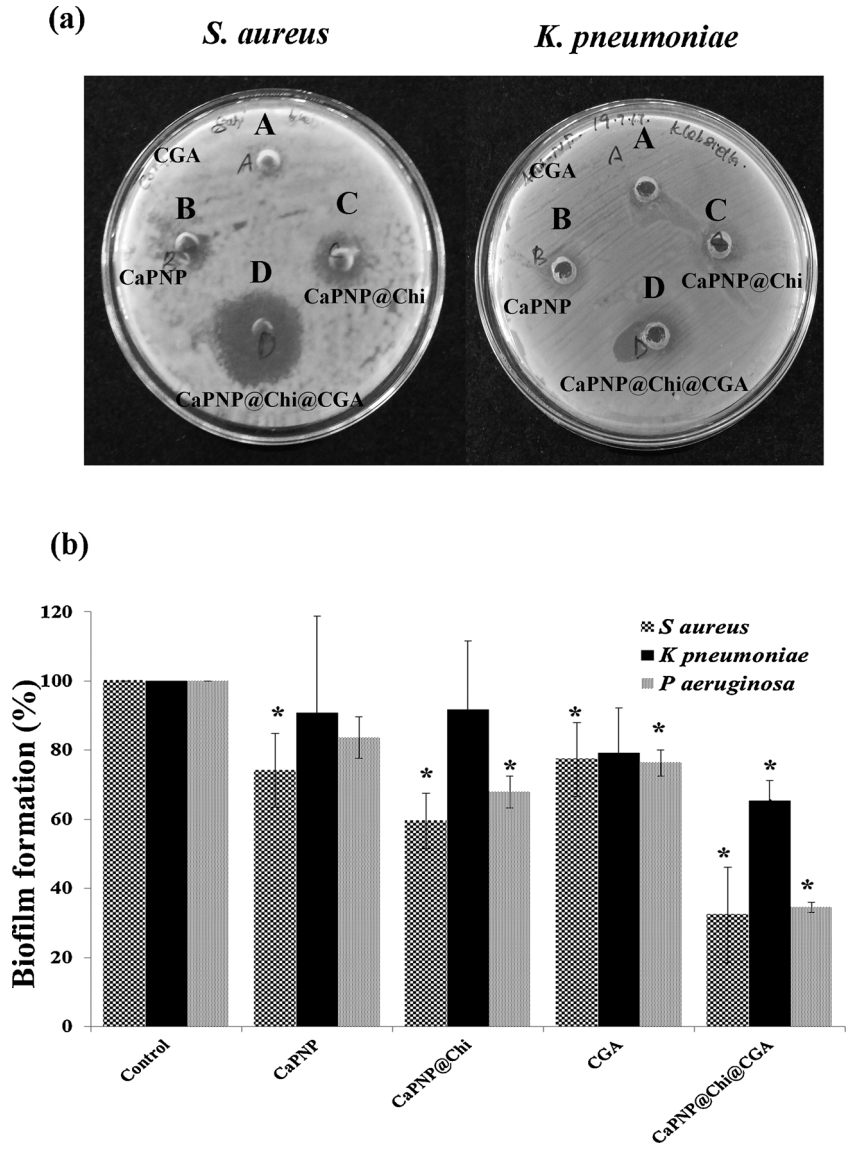

Fig. 5. (a) Antibacterial activity of synthesized nanogel against *S. aureus* and *K. pneumoniae* of (A) CaPNP, (B) CGA, (C) CaPNP@Chi and (D) CaPNP@Chi@CGA by well diffusion method. (b) Biofilm formation assay of synthesized nanogel against *S. aureus K. pneumoniae* and *P. aeruginosa* by crystal **violet** and safranin O staining assay (A) control, (B) CaPNP, (C) CaPNP@Chi, (D) CGA and (E) CaPNP@Chi@CGA. * $P < 0.05$ statistically significant compared with control.

3. Results and discussion

3.1. Characterization of nanogel: Hydrodynamic diameter, zeta potential and SEM analysis

Table. 1 shows the hydrodynamic diameter of uncalcinated (329.3 nm ± 3.6) and calcinated CaPNP (76.3 nm ± 1.4) at pH 7.4. As saliva plays a significant role in demineralization and re-mineralization process, it is vital to entrap the CaPNP in a suitable carrier. pH-dependent flexibility of chitosan facilitates molecular interactions. The stoichiometric ratio of chitosan to crosslinker results in the micro or macroporous structure. The choice of chitosan as a nanocarrier was due to its capability to disrupt bacterial cell membrane (Kumaraswamy et al., 2018) and can result in the release of calcium and phosphate ions to facilitate the re-mineralization process. The hydrodynamic diameter of CaPNP@Chi in PBS buffer at pH 7.4 was found to be 559.6 nm ± 8.5.

Composites of calcium and phosphate ions are very widely used for filling tooth cavities. From dental cavities to dental caries to dental cure the tooth goes through demineralization and re-mineralization process (Zhang et al., 2015),(Abou Neel et al., 2016). The demineralization process is well understood to be caused by the presence of oral pathogenic microbes. Nano-sized calcium phosphate composites dependent re-mineralization process can help the minerals to retain molecular structure of the tooth (Xie et al., 2016). Causative agents of dental cavities are the presence of pathogen and the formation of biofilm. Chitosan nanoparticles entrapped with CGA can inhibit the biofilm formation. Earlier reports indicate that reduction in particle size could be due to the ionic interaction between amine groups of chitosan and charged groups of drug (Seda et al., 2012). The decrease in the hydrodynamic diameter of CaPNP@Chi@CGA (468 nm ± 2.7) when compared with CaPNP@Chi could be due to the electrostatic interaction between chlorogenic acid with CaPNP and chitosan @ pH 7.4, which is noticeable even in saliva mimic @ pH 6.7 (Table 1).

The zeta potentials of uncalcinated and calcinated CaPNP were found to be -7.15 mV ± 0.3 and -11.16 mV ± 0.2 whereas at pH 6.7 there was an decrease in zeta potential to -4.4 mV ± 0.5 and -6.5 mV ± 0.1 respectively. The nanogel of CaPNP@Chi and CaPNP@Chi@CGA in salivary (pH = 6.7) there was an increase in zeta potentials from 8.58 mV ± 0.5 and 7.06 mV ± 0.1 to

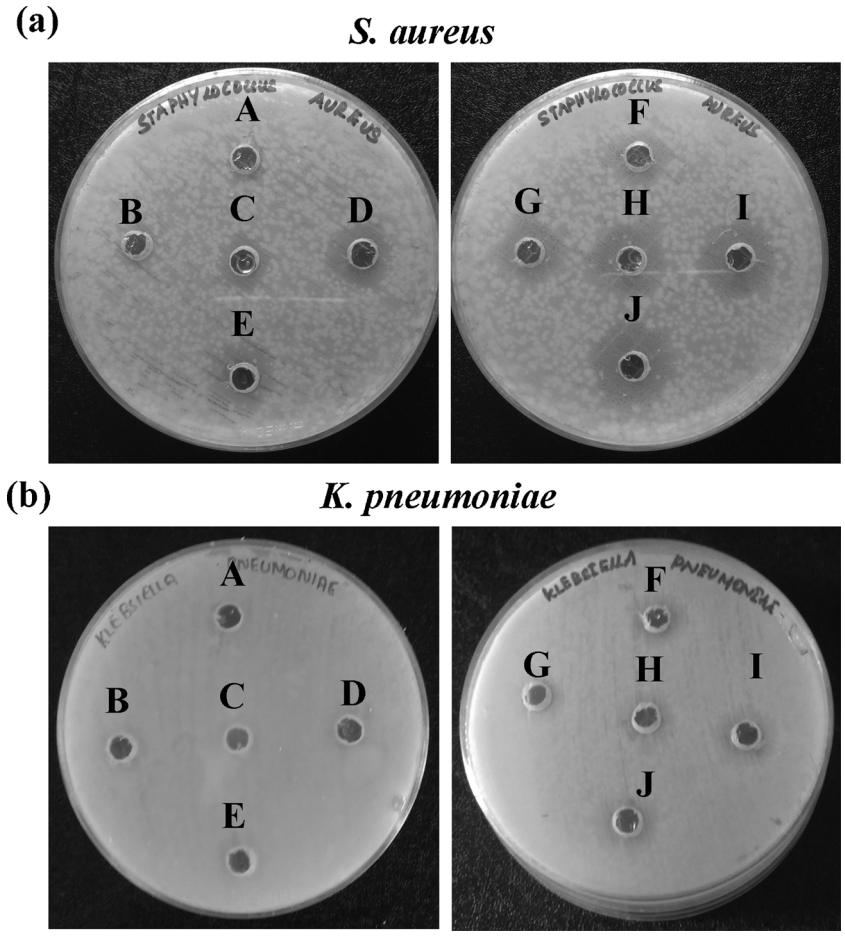

Fig. 6. Antibacterial activity of (A) Control (B) CaPNP and (C–J) CaPNP@Chi@CGA which contains CGA at different concentration (1 μg, 2 μg, 3 μg, 5 μg, 7.5 μg, 10 μg, 12.5 μg, 15 μg) against (a) *S. aureus* and (b) *K. pneumoniae* by well diffusion method.

Table 2
Dose-dependent zone of inhibition against *S. aureus* and *K. pneumoniae* by CaPNP@Chi@CGA using well diffusion method.

Different concentration of CGA used in the nanogel* CaPNP@Chi preparation (μg/mL)	Zone of inhibition (mm) *S aureus K pneumoniae*
1	2.2 ± 0.2 -
2	3.1 ± 0.3 -
3	3.3 ± 0.3 -
5	4.2 ± 0.2 1.6 ± 0.3
7.5	5.7 ± 0.2 2.1 ± 0.3
10	7.7 ± 0.2 1.8 ± 0.2
12.5	9.5 ± 0.4 2.8 ± 0.1
15	11.9 ± 0.1 4.0 ± 0.0

* Amount of nanogel CaPNP@Chi used (35 μg/mL).

Table 3
Zone of inhibition of CGA, CaPNP, CaPNP@Chi and CaPNP@Chi@CGA against *S. aureus* and *K. pneumoniae* using well diffusion method.

Samples	Zone of inhibition (mm)	
	S aureus	*K pneumoniae*
CGA	5.8 ± 0.2	3.5 ± 0.5
CaPNP	7.3 ± 0.5*	2.4 ± 0.5
CaPNP@Chi	11.3 ± 1.0*	7.2 ± 1.0*
CaPNP@Chi@CGA	18.7 ± 0.6*	9.3 ± 1.4*

Amount of CGA used (20 μg/mL) containing (35 μg/mL) of CaPNP@Chi.
* $P < 0.05$ statistically significant when compared to CGA.

20.16 mV ± 0.7 and 18.90 mV ± 0.3, respectively. The positive zeta potential value of CaPNP@Chi indicates entrapment of chitosan. The decreased zeta potential at pH 7.4 when compared to pH 6.7 could be due to the protonation of amine groups in chitosan (Qinna et al., 2015) (Nikpour et al., 2012) or the entrapment and adsorption of CGA on the surface of the nanoparticles (Table 1).

Verma et al. (Verma et al., 2009) synthesized porous scaffolds by adding hydroxyapatite nanoparticles to chitosan/polygalacturonic acid. Sodium tripolyphosphate (TPP) anions are widely used for the preparation of chitosan NPs/gel/scaffold/composites. Gel formation was noticed at 1.25:1 weight ratio of calcium phosphate nanoparticle to chitosan. The use of calcium and phosphate ions as a crosslinker for the formation of CaPNP@Chi nanogel has not been reported. As observed here the negative zeta potential values of CaPNP could be due to the presence of phosphate ions. An attempt was made to prepare nanogel using CaPNP as a crosslinker for the formation of porous structure so that it can, not only help the intermolecular binding of chitosan but can also result in entrapment of CaPNP. The detailed methodology is presented in the Suppl. Fig. 1.

Reports using TPP as a cross linker indicated that techniques like dense gas forming (Ji et al., 2011), sol-gel method (Tripathi and Basu, 2012), dip coating method (In-Kook et al., 2007) polyelectrolyte complexion and freeze drying (Griffon et al., 2006) can result in the formation of porous structure, through Ostwald ripening that can trigger formation of pores. SEM (Fig. 1 and Suppl. Fig. 2) shows the presence of pores in the nanogels of CaPNP@Chi and CaPNP@Chi@CGA. The near equal weight ratio of chitosan to CaPNP could have facilitated intermolecular interactions where in the water molecules could be entrapped within the gel, which on freeze drying can facilitate the

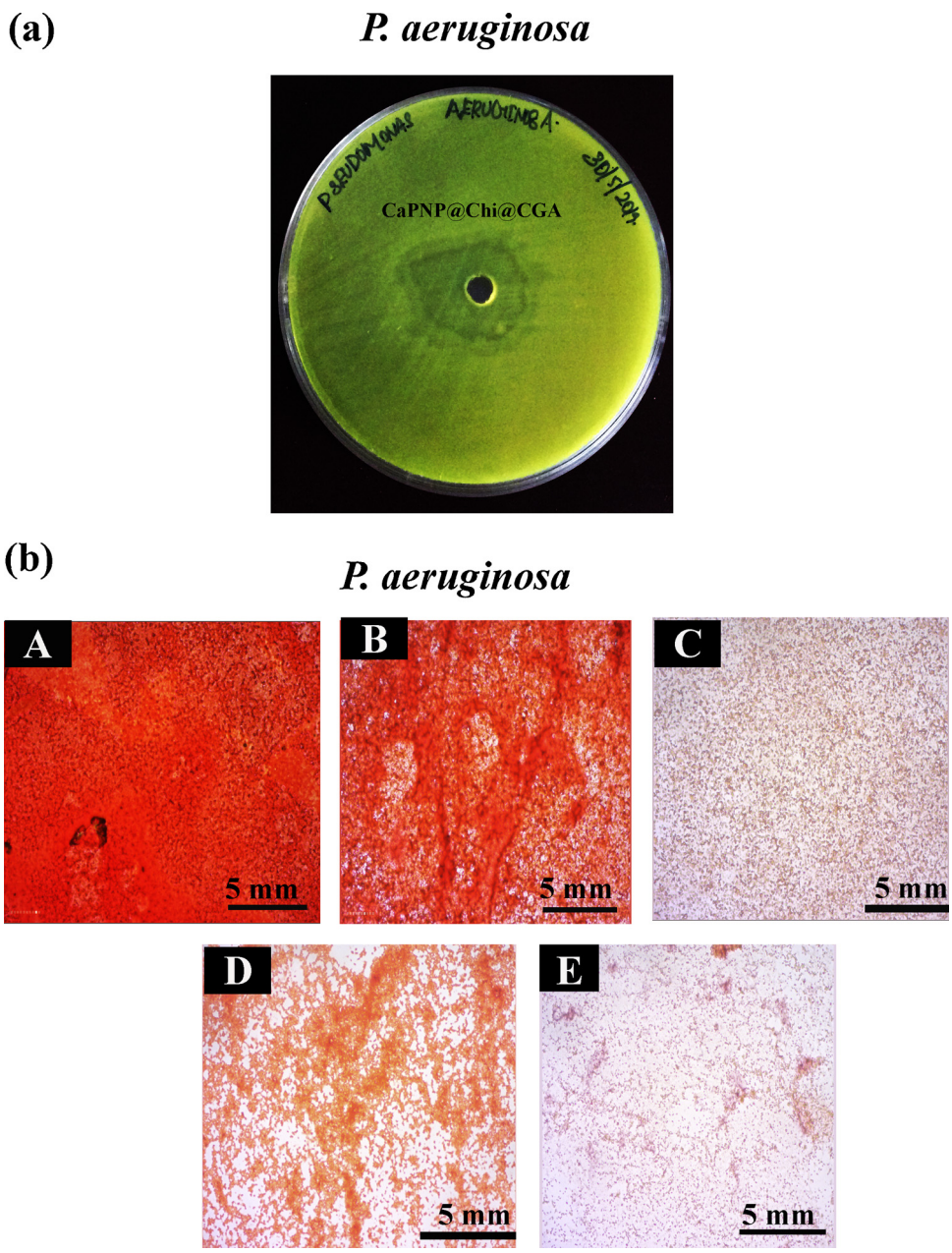

Fig. 7. (a) Antibacterial activity of CaPNP@Chi@CGA (CGA@20 µg) against *P. aeruginosa* by well diffusion method. (b) Optical micrographic images of *P. aeruginosa* biofilm degradation assay of synthesized nanogel by safranin O staining assay (A) control, (B) CaPNP@Chi, (C) CaPNP@Chi, (D) CGA and (E) CaPNP@Chi@CGA at 40 X magnification.

formation of porous scaffold.

3.2. Structural characterization of nanogel: FT IR, XRD, DSC and TGA analysis

Fig. 2b illustrates the FTIR spectra of calcinated calcium phosphate nanoparticle. The details of the changes in the FTIR spectra, matched with reported literature (Lai et al., 2005) are provided as supplementary information. For instance, the changes in asymmetric stretching and bending vibrations of phosphate, absence of OH stretch and carbonate band, a band at 1379 cm^{-1} that is characteristic of amine group – phosphate group interaction, the shift in the peak intensities at 1534 cm^{-1}, 1054 cm^{-1} and 1016 cm^{-1}, the presence of glucosamine stretching vibrations at 1059 cm^{-1} are all indicative of the formation of calcium phosphate-chitosan nanogel with entrapped CGA (Fig. 2c).

Specific bands that are indicative of the formation of calcium phosphate-chitosan nanogel with entrapped CGA have been observed. The broader stretch at 1614 cm^{-1} indicates overlapping of the amide bond with the C=C stretch of chlorogenic acid and the broader stretch of −COOH group at 1750 cm^{-1} also suggest the ionic entrapment of chlorogenic acid in the porous calcium phosphate/chitosan nanogel with the amine group of chitosan (Anuradha et al., 2014; Nallamuthu et al., 2015). The shift in the peak intensities at 1534 cm^{-1}, 1054 cm^{-1} and 1016 cm^{-1} indicates entrapment of chlorogenic acid due to it interaction with phosphate groups of calcium phosphate nanoparticles and amine groups of chitosan (Fig. 2c).

Chlorogenic acid incorporated CaPNP@Chi was amorphous in character, as revealed by XRD spectra (Fig. 3). CaPNP are crystalline in nature and chitosan NP are amorphous in nature, and complexion and incorporation of polymer can result in the loss of crystallinity (Willi and P., 2010) resulting in broad peaks (Manatunga et al., 2016) in the XRD pattern of CaPNP@Chi@CGA (Fig. 3). Venkatesan et al. (Venkatesan

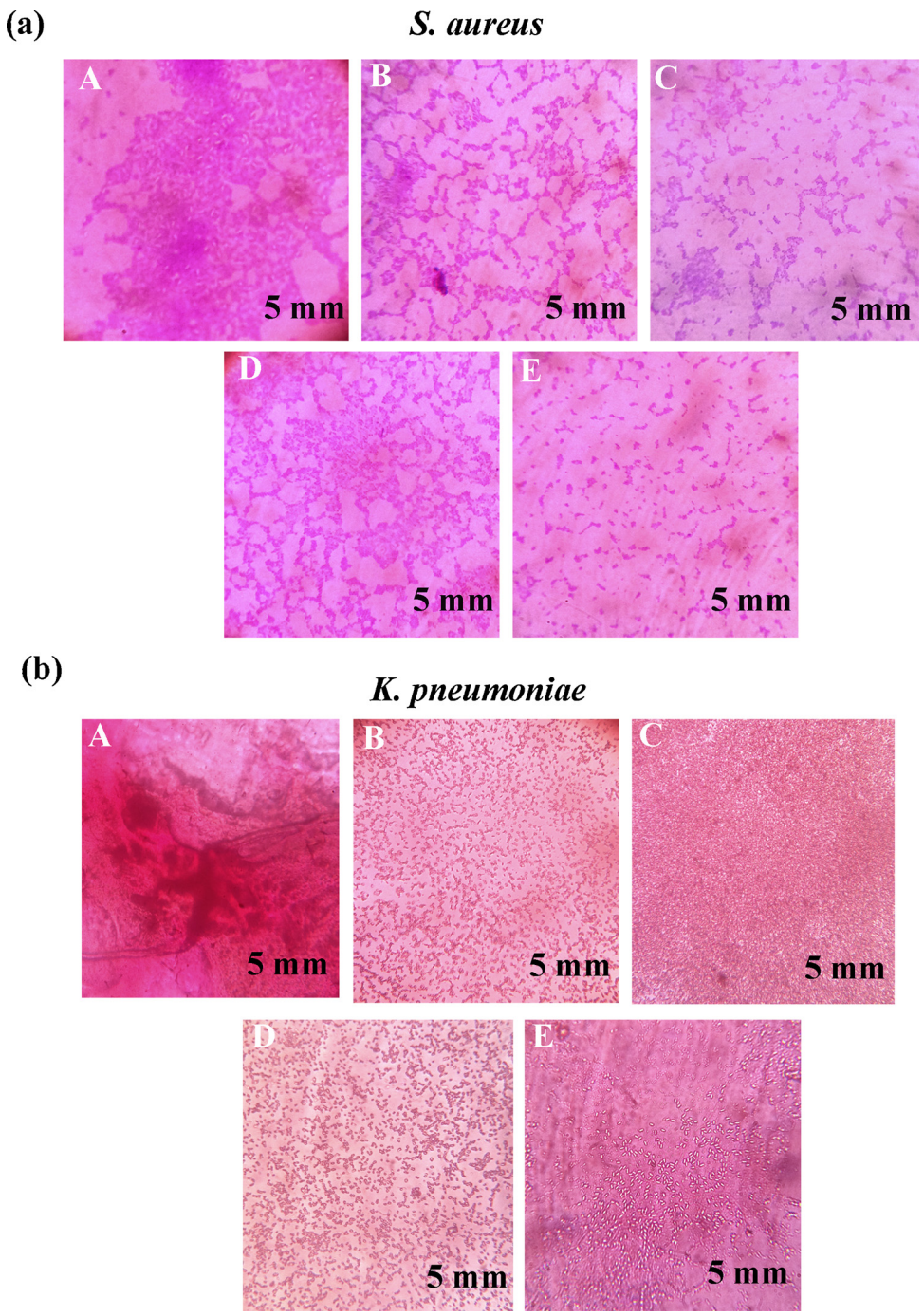

Fig. 8. Optical micrographic images of (a) *S. aureus* and (b) *K. pneumoniae* biofilm degradation assay of synthesized nanogel by crystal **violet** and safranin O staining assay (A) control, (B) CaPNP@Chi, (C) CaPNP@Chi, (D) CGA and (E) CaPNP@Chi@CGA at 40 X magnification.

et al., 2012) suggested that amorphous character can be due to the formation of pores.

It is important to understand the decomposition of materials especially for dental applications since materials can encounter various thermal process during intake and digestion of food. In this study, the sharp endothermic peak observed in the DSC study of CGA (Fig. 4a) is considered as the melting point of CGA. CaPNP@Chi nanogel showed an endothermic peak at 93.0 °C, which on interaction with CGA is shifted to 100.3 °C indicating the interaction of CGA with chitosan (Rogina et al., 2013). Melting point of CGA or endothermic peak at 211 °C disappeared in CaPNP@Chi establishing the incorporation of CGA, an observation similar to that made by Zhang et al. (Yuying et al., 2008). This information aids in understanding the structural stability of synthesized nanomaterials.

To understand the weight difference of materials TGA analysis was carried out (Lin et al., 2014). TGA of chlorogenic acid (Fig. 4b) indicates at least 5 decomposition patterns at 69.0 °C, 200.2 °C, 301.8 °C, 398.8 °C and 612.6 °C, four of which are close to earlier reports (Owusu-Ware et al., 2013) (Wei et al., 2011) (Sharma et al., 2002). In our study, a fifth decomposition step is observed at 612 °C for CGA. CaPNP synthesized with the ratio of 1.33 indicated most of the degradation pattern below 600 °C. Earlier studies on CaPNP/polymer conjugated with fluorescent dye had a decomposition temperature between 200–600 °C (Schwiertz et al., 2009), (Kim et al., 2008). In this study CaPNP@Chi@CGA decomposition pattern was observed at 124.4 °C, 247.2 °C, 387.5 °C and 568.7 °C. The thermal stability of the gel is confirmed by

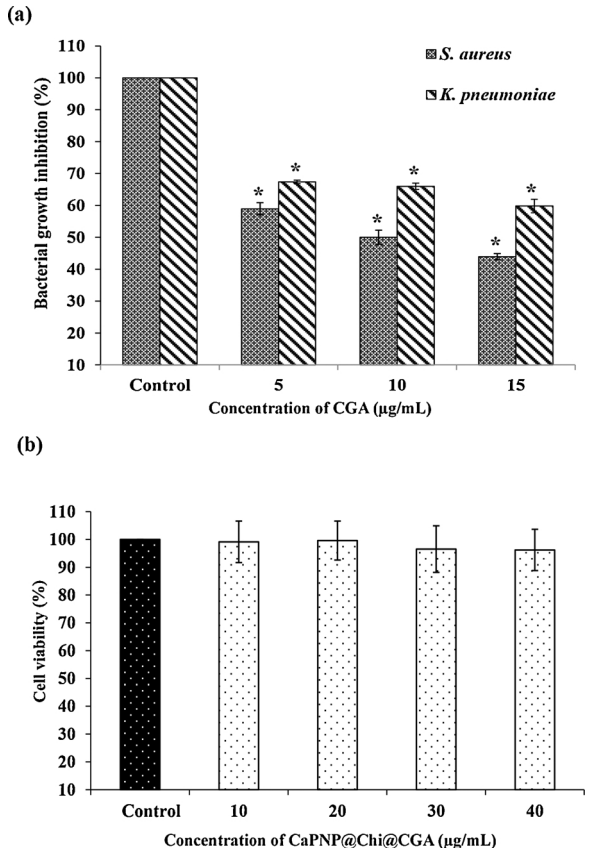

Fig. 9. (a) Bacterial growth inhibition of CGA at different concentration 5, 10 and 15 µg/mL (b) Cell viability of CaPNP@Chi@CGA at different concentration 10, 20, 30 and 40 µg/mL by MTT assay on HaCaT cell line. * $P < 0.05$ statistically significant compared to control.

this experiment. Characterization techniques cumulatively suggest that a porous nanogel of CaPNP@Chi@CGA was formed.

3.3. Antibacterial, biofilm degradation of nanogel

The main causative factor for cavity formation as described earlier is due to the acid attack by cariogenic bacteria. Among oral pathogens, *S. aureus* and *K. pneumoniae* are opportunistic pathogens (K, K et al., 2009) which can colonize the mouth (Terpenning et al., 2001). Fig. 5a indicates better growth inhibition by CaPNP@Chi@CGA as compared to other nanoparticles against gram positive and gram negative bacteria. Fig. 6 and Table 2 provide information on bacterial growth inhibition of CaPNP@Chi loaded with different concentration of CGA varying from 1 to 15 µg/mL against *S. aureus* and *K. pneumoniae*. The growth inhibition of CaPNP@Chi@CGA, having a positive zeta potential, was more against gram positive than gram negative bacteria. Fig. 5a and Table 3 provides information on zone of inhibition values for CaPNP@Chi containing 20 µg/mL of CGA was compared with 20 µg/mL of CGA and 35 µg/mL of CaPNP@Chi. An earlier report on minimum inhibitory concentration of chitosan, chitosan nanoparticles and chlorogenic acid against different bacterial species is indicated in Suppl. Table 1. The CaPNP@Chi entrapped with CGA inhibited bacterial growth to greater extent when compared with CaPNP and CGA alone against *S. aureus* which was found to be 18.7 mm ± 0.6 (Table 3). For *K. pneumoniae* and *P. aeruginosa,* the zone of inhibition of CaPNP@Chi@CGA was found to be 9.30 mm ± 1.36 (Table 3) and 16.7 mm ± 0.83 (Fig. 7a) respectively. NP with positive surface charge can interact with negatively charged bacteria resulting in inhibition of bacterial growth (Shi et al., 2016). In this study the nanogel formed was CaPNP and chitosan. Inhibition of gram positive *S. aureus* could be *via* interaction with negatively charged CaPNP, there by disrupting the cell membrane. The inhibition of gram negative *K. pneumonia*e could be *via* interaction with positively charged of chitosan. The negatively charged dentin surface can interact with CaPNP@Chi@CGA through electrostatic interactions and also inhibit growth of bacteria.

Fig. 5b provides information about antibiofilm activity of CaPNP@Chi@CGA performed by crystal violet staining assay for *S. aureus*; safranin O staining for *K. pneumoniae* and *P.aeruginosa*. At the amount of 20 µg/mL of CGA CaPNP@Chi@CGA used, there was a significant change of $p < 0.05$ for all the groups when compared with the control against *S. aureus.* CaPNP@Chi@CGA provided 68% degradation of biofilm when compared with the control group. The corresponding values were 41% and 23% for CaPNP@Chi nanogel and CGA alone respectively. This could be due to the interaction of negative charged CaPNP against positive charge *S. aureus.* The greater extent of inhibition of biofilm by CaPNP@Chi@CGA on *S. aureus* could be due to the presence of CaPNP that could have helped in the interaction of gel with biofilm while the presence of CGA in scaffold help in the reduction of formation of biofilm against *S. aureus.* The porous structure of chitosan scaffolds could slowly release the entrapped CGA and thus inhibit or disrupt the membrane integrity of *K. pneumoniae* there by resulting in cell death. In this study the biofilm was washed with buffer solution. Hence there is a chance of unbound particles to be washed off. The charge of CaPNP in binding to the biofilm of gram positive bacteria could have played a crucial role in significant inhibition of biofilm against *S. aureus.* The porous structure of the nanogel could have contributed to a greater extent of biofilm inhibition. The optical micrograph images of *P. aeruginosa*, *S. aureus* and *K. Pneumoniae* biofilm degradation stained by safranin O and crystal violet is shown in Fig. 7b; Fig. 8a and Fig. 8b respectively.

Biofilm formation on dental surfaces can lead to infection and the way is to eradicate this menace is to remove the tooth. Researchers worldwide are currently looking at the mechanism to regenerate the tooth so as to avoid its removal and prevent formation of biofilm. CaPNP@Chi@CGA nanogel showed a promising inhibition of growth of gram positive and gram negative bacteria. To understand the structural morphology of bacterial cells after the exposure of CaPNP@Chi@CGA, HRSEM analysis was performed with three organisms *Staphylococcus aureus, Klebsiella pneumoniae* and *Pseudomonas aeruginosa*. Bacterial cells were grown on cover slips and treated with CaPNP@Chi@CGA for 6 h and untreated cells were incubated under same conditions. Fixed bacterial cells were collected for HRSEM analysis (Fig. 10a). HR SEM provides information about cell membrane damage of drugs against biofilm – bacteria. To understand biocidal activity of CaPNP@-Chi@CGA, in this study a time course analysis was carried out. Fig. 10a A–C reveals the bacterial cellular morphology of cells treated and not treated with CaPNP@Chi@CGA for 6 h. Morphology clearly indicates that the bacterial cells treated with CaPNP@Chi@CGA lost membrane integrity during the formation of biofilm. It is interesting to note that biocidal activity was found in all three microorganisms used in this study. The first defense mechanism for treating is to eradicate the biofilm formation. As microorganisms are involved in demineralization process it is pivotal to disrupt the well-organized architecture of biofilm formation. The loss of well-organized architecture of biofilm could be due to the multifunctional mode of compounds. Extracellular polysaccharide (EPS) mainly lipids, proteins and polysaccharides plays a major role in the formation of biofilm. Chitosan being positive charge can bind to the negative charge of EPS (Pearce, 1973). CaPNP not only acts in damaging the bacterial cell membrane architecture but also increase the sorption process due to the change in the membrane efflux pump caused by CaPNP. Chitosan is a well-known antimicrobial agent and is known to penetrate the biofilm and inhibit biofilm formation. The amine group of chitosan can bind with the negative charge of EPS layer and can also disrupt the biofilm formation. Chitosan can alter the bacterial metabolism there by preventing the growth of the bacteria by leading to destabilization of cell membrane (Rakesh et al., 2018) that

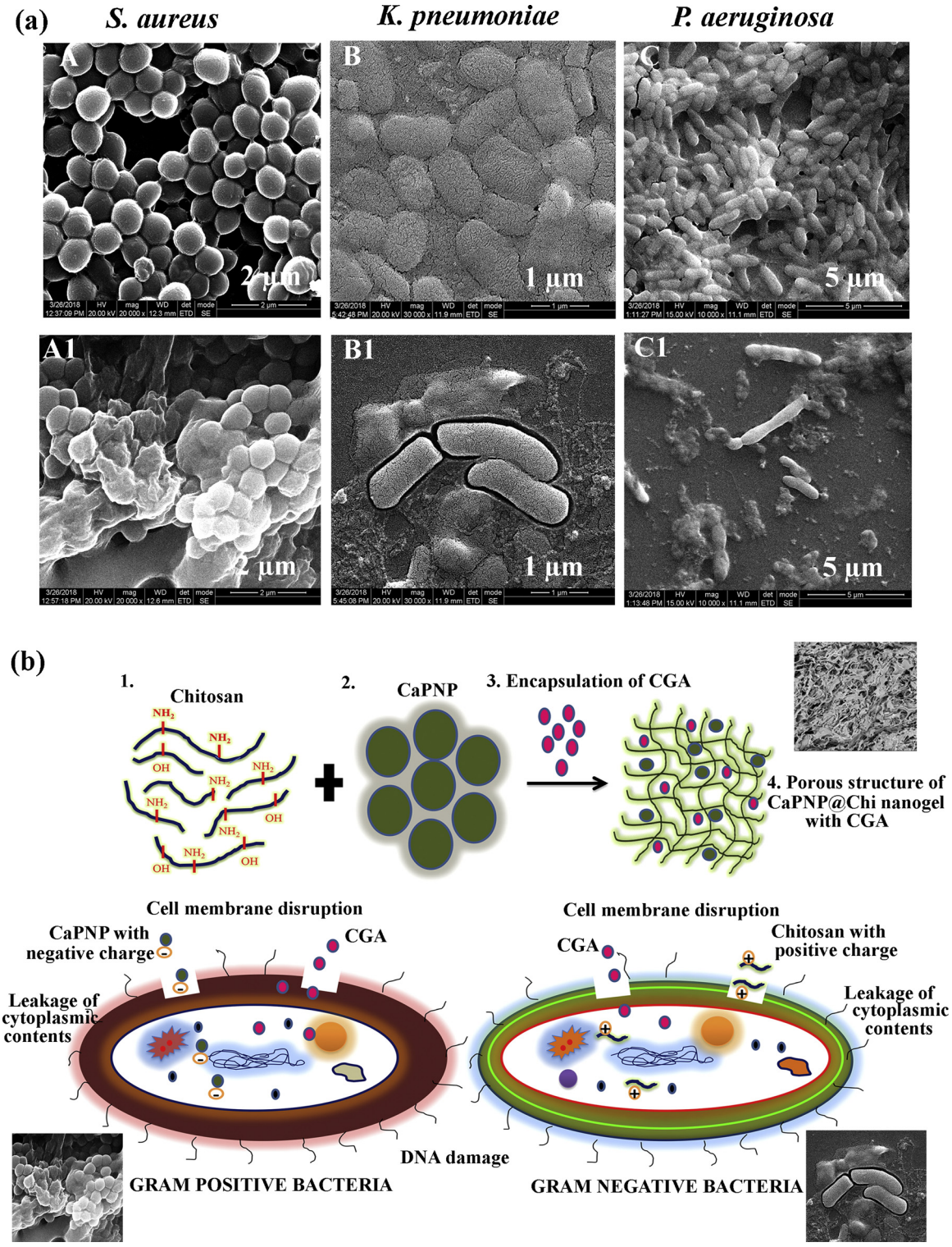

Fig. 10. (a) Bacterial cellular morphology of *S. aureus* (A) control and (A1) treated with CaPNP@Chi@CGA (20,000 X magnification), *K. pneumoniae* (B) control and (B1) treated with CaPNP@Chi@CGA (30,000 X magnification), *P. aeruginosa* (C) control (C1) treated with CaPNP@Chi@CGA (10,000 X magnification) by HR SEM analysis. (b) Mechanism of CaPNP@Chi@CGA against gram positive and gram negative bacteria.

can in turn lead to cell lysis. In another mechanism DNA function would be inhibited by the binding of chitosan with the phosphate groups of DNA which is negatively charged. The addition of CGA in the porous nanogel results in bacterial cell death by tapping the membrane function there by releasing cytoplasmic contents of bacteria (Kumaraswamy et al., 2018). With increased menace of multi drug resistance of bacteria, it is important to surprise the bacteria by multifunctional approach (Kumaraswamy et al., 2018). Detailed mechanism of CaPNP@Chi@CGA nanogel on biofilm degradation, bacterial growth/inhibition is presented in Fig. 9a and 10 b. The plausible mechanism for the action of the nanogel is based on the interplay of surface charges. The synthesis design ensures that each component of the nanogel has its own charged sites still available for reaction. Accordingly, it is presumed that the positive charge of chitosan would enable to react with

gram negative bacteria (Helander et al., 2001) and in a similar way the abundance presence of negative charge on gram positive bacteria (Liu et al., 2013) can interact with the nanogel and the negatively charged phosphate ions of calcium phosphate would interact with the components of gram positive bacteria (Iqbal et al., 2014). This interaction between the bacteria and the oppositely charged ions in the nanogel ensures the bacterial elimination in the surface of dentine. Studies on the sustained release of the drug from the porous structure of the calcium phosphate chitosan nanogel are underway. The drug chosen and the chitosan can disrupt the cell membrane, influence the plasma membrane and permeate through the cell, which in turn can lead to leakage of cytoplasmic contents and inhibit growth of the bacteria, thus degrade the biofilms and alter the DNA functions, thus eliminating carries.

3.4. Cell viability studies

The use of CaPNP@Chi@CGA nanogel warrants understanding toxicity of nanogel on healthy cells. In our study, we used human keratinocyte cell line (HaCaT) to understand whether CaPNP@Chi@CGA can interfere with cell membrane damage. MTT assay was performed to examine the cytotoxicity of HaCaT cells treated with various concentrations of CaPNP@Chi@CGA, ranging from 10 to 40 µg/mL for 18 h (Fig. 9b). These results were non-significant when compared with the control group. CGA is not well adsorbed in rats (Azuma et al., 2000), and thus, formulations, which can help in adsorption, are required. Cell viability and morphology of nanoporous gel did not show toxicity in HaCaT cell lines until the concentration of 40 µg/mL. CGA protects HUVEC against peroxide damage in a dose-dependent manner (0.1 to 10 µg/mL) (Wu et al., 2012). Chitosan and CaPNP are known to be protective against human keratinocyte cells, osteoblast-like human cells, human dermal micro vascular endothelial cells, primary human osteoblasts, and its toxicity is mainly dependent on physicochemical properties and cell types. The results indicated that CaPNP@Chi@CGA did not cause toxicity to cells up to 40 µg/mL.

4. Conclusion

Taking note of the dependency of periodontal diseases and dental caries on bacterial biofilms that remain adhered to the teeth and a need to prevent from acid promoted secondary caries, this work has been designed to develop a nanogel that provides a porous structure for controlled drug release, biocompatibility to the protein structure in the dentine, elimination of bacterial growth and its subsequent growth. An ionic gelation method with calcium phosphate nanoparticle as cross-linker formed the base of the nanostructure. The presence of negative charge on phosphate ions and a positive charge on chitosan enabled the neutralization of bacterial growth. Chitosan and CGA could disrupt the bacterial cell membrane and permeate through the cell, thus eliminating the biofilm formation. The nanogel design enables further encapsulation of agents that can promote odontoblast differentiation of mesenchymal stem cells from human dental pulp, in the future.

Acknowledgement

SP thanks, Lady Tata Memorial Trust for JRF. This work was financially supported by Chettinad Academy of Research and Education, Tamil Nadu, India. We thank CSIR-CLRI for instrumentation facilities.

Appendix A. Supplementary data

Supplementary material related to this article can be found, in the online version, at doi:https://doi.org/10.1016/j.biocel.2019.105566.

References

Abou Neel, E.A., Aljabo, A., Strange, A., Ibrahim, S., Coathup, M., Young, A.M., Bozec, L., Mudera, V., 2016. Demineralization–remineralization dynamics in teeth and bone. Int. J. Nanomedicine 11, 4743–4763.
Aijun, W., Qiang, A., Wenling, C., Mingzhi, Y., Qing, H., Lijun, K., Ling, Z., Yandao, G., Xiufang, Z., 2006. Porous chitosan tubular scaffolds with knitted outer wall and controllable inner structure for nerve tissue engineering. J. Biomed. Mater. Res. A. 79A (1), 36–46.
Anuradha, Chandra Joshi, J., Gulati, K., Ray, A., Roy, I., 2014. Fluorophore-doped calcium phosphate nanoparticles for non-toxic biomedical applications. RSC Adv. 4 (76), 40449–40455.
Azuma, K., Ippoushi, K., Nakayama, M., Ito, H., Higashio, H., Terao, J., 2000. Absorption of chlorogenic acid and caffeic acid in rats after oral administration. J. Agric. Food Chem. 48 (11), 5496–5500.
Baidamshina, D.R., Trizna, E.Y., Holyavka, M.G., Bogachev, M.I., Artyukhov, V.G., Akhatova, F.S., Rozhina, E.V., Fakhrullin, R.F., Kayumov, A.R., 2017. Targeting microbial biofilms using Ficin, a nonspecific plant protease. Sci. Rep. 7, 46068.
Chen, H., Zhang, X., Dai, S., Ma, Y., Cui, S., Achilefu, S., Gu, Y., 2013. Multifunctional gold nanostar conjugates for tumor imaging and combined photothermal and chemotherapy. Theranostics 3 (9), 633–649.
Cheng, L., Weir, M.D., Zhang, K., Wu, E.J., Xu, S.M., Zhou, X., Xu, H.H., 2012. Dental plaque microcosm biofilm behavior on calcium phosphate nanocomposite with quaternary ammonium. Dent. Mater. 28 (8), 853–862.
Danilchenko, S.N., Kalinkevich, O.V., Pogorelov, M.V., Kalinkevich, A.N., Sklyar, A.M., Kalinichenko, T.G., Ilyashenko, V.Y., Starikov, V.V., Bumeyster, V.I., Sikora, V.Z., Sukhodub, L.F., 2011. Characterization and in vivo evaluation of chitosan-hydroxyapatite bone scaffolds made by one step coprecipitation method. J. Biomed. Mater. Res. A. 96 (4), 639–647.
Dias, H.B., Bernardi, M.I.B., Bauab, T.M., Hernandes, A.C., de Souza Rastelli, A.N., 2019. Titanium dioxide and modified titanium dioxide by silver nanoparticles as an anti biofilm filler content for composite resins. Dent. Mater. 35 (2), e36–e46.
Fan, W., Yan, W., Xu, Z., Ni, H., 2012. Formation mechanism of monodisperse, low molecular weight chitosan nanoparticles by ionic gelation technique. Colloids Surf. B Biointerfaces 90, 21–27.
Griffon, D.J., Sedighi, M.R., Schaeffer, D.V., Eurell, J.A., Johnson, A.L., 2006. Chitosan scaffolds: interconnective pore size and cartilage engineering. Acta Biomater. 2 (3), 313–320.
Helander, I.M., Nurmiaho-Lassila, E.L., Ahvenainen, R., Rhoades, J., Roller, S., 2001. Chitosan disrupts the barrier properties of the outer membrane of gram-negative bacteria. Int. J. Food Microbiol. 71 (2-3), 235–244.
In-Kook, J., Ju-Ha, S., Won-Young, C., Young-Hag, K., Hyoun-Ee, K., Hae-Won, K., 2007. Porous hydroxyapatite scaffolds coated with bioactive apatite–Wollastonite glass–Ceramics. J. Am. Ceram. Soc. 90 (9), 2703–2708.
Iqbal, N., Kadir, M.R.A., Mahmood, N.H., Salim, N., Froemming, G.R.A., Balaji, H.R., Kamarul, T., 2014. Characterization, antibacterial and in vitro compatibility of zinc–silver doped hydroxyapatite nanoparticles prepared through microwave synthesis. Ceram. Int. 40 (3), 4507–4513.
Ji, C., Annabi, N., Khademhosseini, A., Dehghani, F., 2011. Fabrication of porous chitosan scaffolds for soft tissue engineering using dense gas CO2. Acta Biomater. 7 (4), 1653–1664.
K, K, A, D.T, T, O, 2009. Increase in detectable opportunistic bacteria in the oral cavity of orthodontic patients. Int. J. Dent. Hyg. 7 (2), 121–125.
Kim, S.E., Choi, H.W., Lee, H.J., Chang, J.H., Choi, J., Kim, K.J., Lim, H.J., Jun, Y.J., Lee, S.C., 2008. Designing a highly bioactive 3D bone-regenerative scaffold by surface immobilization of nano-hydroxyapatite. J. Mater. Chem. 18 (41), 4994–5001.
Kumaraswamy, R.V., Kumari, S., Choudhary, R.C., Pal, A., Raliya, R., Biswas, P., Saharan, V., 2018. Engineered chitosan based nanomaterials: bioactivities, mechanisms and perspectives in plant protection and growth. Int. J. Biol. Macromol. 113, 494–506.
Lai, C., Tang, S.Q., Wang, Y.J., Wei, K., 2005. Formation of calcium phosphate nanoparticles in reverse microemulsions. Mater. Lett. 59 (2-3), 210–214.
Lin, P.-C., Lin, S., Wang, P.C., Sridhar, R., 2014. Techniques for physicochemical characterization of nanomaterials. Biotechnol. Adv. 32 (4), 711–726.
Liu, L., Yang, J., Xie, J., Luo, Z., Jiang, J., Yang, Y.Y., Liu, S., 2013. The potent antimicrobial properties of cell penetrating peptide-conjugated silver nanoparticles with excellent selectivity for Gram-positive bacteria over erythrocytes. Nanoscale 5 (9), 3834–3840.
Lou, Z., Wang, H., Zhu, S., Ma, C., Wang, Z., 2011. Antibacterial activity and mechanism of action of chlorogenic acid. J. Food Sci. 76 (6), M398–403.
Manatunga, D.C., de Silva, R., de Silva, K.M.N., Ratnaweera, R., 2016. Natural polysaccharides leading to super adsorbent hydroxyapatite nanoparticles for the removal of heavy metals and dyes from aqueous solutions. RSC Adv. 6 (107), 105618–105630.
Melo, M.A.S., Weir, M.D., Rodrigues, L.K.A., Xu, H.H.K., 2013. Novel calcium phosphate nanocomposite with caries-inhibition in a human in situ model. Dent. Mater. 29 (2), 231–240.
Nallamuthu, I., Devi, A., Khanum, F., 2015. Chlorogenic acid loaded chitosan nanoparticles with sustained release property, retained antioxidant activity and enhanced bioavailability. Asian J. Pharm. Sci. 10 (3), 203–211.
Nikpour, M.R., Rabiee, S.M., Jahanshahi, M., 2012. Synthesis and characterization of hydroxyapatite/chitosan nanocomposite materials for medical engineering applications. Composites Part B-Engineering 43 (4), 1881–1886.
Ommen, P., Zobek, N., Meyer, R.L., 2017. Quantification of biofilm biomass by staining: non-toxic safranin can replace the popular crystal violet. J. Microbiol. Methods 141, 87–89.
Owusu-Ware, S.K., Chowdhry, B.Z., Leharne, S.A., Antonijevic, M.D., 2013. Quantitative

analysis of overlapping processes in the non-isothermal decomposition of chlorogenic acid by peak fitting. Thermochim. Acta 565, 27–33.
Pearce, E.I.F., 1973. Adsorption by hydroxyapatite of extracellular polysaccharides produced by various strains of oral streptococci. J. Dent. Res. 52 (3), 574–575.
Pepla, E., Besharat, L.K., Palaia, G., Tenore, G., Migliau, G., 2014. Nano-hydroxyapatite and its applications in preventive, restorative and regenerative dentistry: a review of literature. Ann. Stomatol. (Roma) 5 (3), 108–114.
Petti, S., Scully, C., 2009. Polyphenols, oral health and disease: a review. J. Dent. 37 (6), 413–423.
Qinna, N.A., Karwi, Q.G., Al-Jbour, N., Al-Remawi, M.A., Alhussainy, T.M., Al-So'ud, K.A., Al Omari, M.M.H., Badwan, A.A., 2015. Influence of Molecular Weight and Degree of Deacetylation of Low Molecular Weight Chitosan on the Bioactivity of Oral Insulin Preparations. Mar. Drugs 13 (4), 1710–1725.
Rakesh, K.P., Vivek, H.K., Manukumar, H.M., Shantharam, C.S., Bukhari, S.N.A., Qin, H.-L., Sridhara, M.B., 2018. Promising bactericidal approach of dihydrazone analogues against bio-film forming Gram-negative bacteria and molecular mechanistic studies. RSC Adv. 8 (10), 5473–5483.
Rogina, A., Ivankovic, M., Ivankovic, H., 2013. Preparation and characterization of nano-hydroxyapatite within chitosan matrix. Mater. Sci. Eng. C Mater. Biol. Appl. 33 (8), 4539–4544.
Roohani-Esfahani, S.-I., Newman, P., Zreiqat, H., 2016. Design and fabrication of 3D printed scaffolds with a mechanical strength comparable to cortical bone to repair large bone defects. Sci. Rep. 6, 19468.
Scannapieco, F.A., Mylotte, J.M., 1996. Relationships between periodontal disease and bacterial pneumonia. J. Periodontol. 67 (10 Suppl), 1114–1122.
Schwiertz, J., Wiehe, A., Grafe, S., Gitter, B., Epple, M., 2009. Calcium phosphate nanoparticles as efficient carriers for photodynamic therapy against cells and bacteria. Biomaterials 30 (19), 3324–3331.
Seda, R., Aydın, T., Pulat, M., 2012. 5-fluorouracil encapsulated chitosan nanoparticles for pH-Stimulated drug delivery: evaluation of controlled release kinetics. J. Nanomater. 2012, 10.
Shamaila, S., Zafar, N., Riaz, S., Sharif, R., Nazir, J., Naseem, S., 2016. Gold nanoparticles: an efficient antimicrobial agent against enteric bacterial human pathogen. Nanomaterials Basel (Basel) 6 (4).
Sharma, R.K., Fisher, T.S., Hajaligol, M.R., 2002. Effect of reaction conditions on pyrolysis of chlorogenic acid. J. Anal. Appl. Pyrolysis 62 (2), 281–296.
Shi, S.-f., Jia, J.-f., Guo, X.-k., Zhao, Y.-p., Chen, D.-s., Guo, Y.-y., Zhang, X.-l., 2016. Reduced Staphylococcus aureus biofilm formation in the presence of chitosan-coated iron oxide nanoparticles. Int. J. Nanomedicine 11, 6499–6506.
Terpenning, M.S., Taylor, G.W., Lopatin, D.E., Kerr, C.K., Dominguez, B.L., Loesche, W.J., 2001. Aspiration pneumonia: dental and oral risk factors in an older veteran population. J. Am. Geriatr. Soc. 49 (5), 557–563.
Tove, L., Nils-Erik, F., 2017. Dental biofilm infections – an update. APMIS 125 (4), 376–384.
Tripathi, G., Basu, B., 2012. A porous hydroxyapatite scaffold for bone tissue engineering: physico-mechanical and biological evaluations. Ceram. Int. 38 (1), 341–349.
Venkatesan, J., Kim, S.K., 2014. Nano-hydroxyapatite composite biomaterials for bone tissue engineering–a review. J. Biomed. Nanotechnol. 10 (10), 3124–3140.
Venkatesan, J., Pallela, R., Bhatnagar, I., Kim, S.K., 2012. Chitosan-amylopectin/hydroxyapatite and chitosan-chondroitin sulphate/hydroxyapatite composite scaffolds for bone tissue engineering. Int. J. Biol. Macromol. 51 (5), 1033–1042.
Verma, D., Katti, K.S., Katti, D.R., 2009. Polyelectrolyte-complex nanostructured fibrous scaffolds for tissue engineering. Materials Science & Engineering C-Materials for Biological Applications 29 (7), 2079–2084.
Wang, H., Ren, D., 2017. Controlling Streptococcus mutans and Staphylococcus aureus biofilms with direct current and chlorhexidine. AMB Express 7 (1), 204.
Wang, J., Liu, G., Chen, J., Zhao, B., Zhu, P., 2015. Synthesis of biocompatible hydroxyapatite using chitosan oligosaccharide as a template. Materials 8 (12), 8097–8105.
Wei, Y., Gao, Y., Xie, Q., Zhang, G., Fu, W., 2011. Isolation of chlorogenic acid from Flaveria bidentis (L.) Kuntze by CCC and synthesis of chlorogenic acid-intercalated layered double hydroxide. Chromatographia 73 (1), 97–102.
Willi, P., P., S.C, 2010. Fatty acid conjugated calcium phosphate nanoparticles for protein delivery. Int. J. Appl. Ceram. Technol. 7 (2), 129–138.
Wu, X., Lin, S., Zhang, X., 2012. Antioxidant and Antiapoptotic Properties of Chlorogenic Acid on Human Umbilical Vein Endothelial Cells.
Xie, X.-J., Xing, D., Wang, L., Zhou, H., Weir, M.D., Bai, Y.-X., Xu, H.H.K., 2016. Novel rechargeable calcium phosphate nanoparticle-containing orthodontic cement. Int. J. Oral Sci. 9, 24.
Yiwen, Z., Hongcai, Z., Shunsheng, C., Hao, F., Yanyun, Z., 2018. Microwave-assisted degradation of chitosan with hydrogen peroxide treatment using Box-Behnken design for enhanced antibacterial activity. Int. J. Food Sci. Technol. 53 (1), 156–165.
Yuying, Z., Yan, Y., Kai, T., Xing, H., Guolin, Z., 2008. Physicochemical characterization and antioxidant activity of quercetin-loaded chitosan nanoparticles. J. Appl. Polym. Sci. 107 (2), 891–897.
Zaltsman, N., Ionescu, A.C., Weiss, E.I., Brambilla, E., Beyth, S., Beyth, N., 2017. Surface-modified nanoparticles as anti-biofilm filler for dental polymers. PLoS One 12 (12), e0189397.
Zhang, L., Weir, M.D., Hack, G., Fouad, A.F., Xu, H.H.K., 2015. Rechargeable dental adhesive with calcium phosphate nanoparticles for long-term ion release. J. Dent. 43 (12), 1587–1595.